International Journal of Botany Studies
ISSN: 2455-541X; Impact Factor: RJIF 5.12
Received: 09-11-2020; Accepted: 23-11-2020: Published: 09-12-2020
www.botanyjournals.com
Volume 5; Issue 6; 2020; Page No. 768-772

Biocompatible *Cicer arietinum* seeds assisted MgO NPs for antibacterial and photocatalytic dye degradation

J Thanuja, H Raja Naika
Department of Studies and Research in Biotechnology, Tumkur University, Tumakuru, Karnataka, India

Abstract
Magnesium oxide nanoparticles were synthesized using magnesium nitrate and *Cicer arientinum* as a fuel via a simple and eco-friendly solution combustion technique. XRD, FTIR, UV-DRS, SEM and EDAX have characterized the structure and morphology of the substance. XRD indicates that the prepared product belongs to the cubic phase system, the average crystallite size of 14 nm. In FTIR, the band at 551 cm^{-1} was indicates the Mg- O bonding. SEM photos showed that the Particles were agglomerated and the structure of a sponge was created. Characterized nanoparticles were subjected to degrade MB dye, photocatalytic and biological (antimicrobial) activities. Bactericidal efficacy was evaluated against *Klebsiella aerogenes*, *E. coli*, and *s. aureus (Staphylococcus aureus)* was exhibited by MgO NPs. By using the agar well diffusion method.

Keywords: MGO nanoparticles, UV- Drs, antibacterial activity, photocatalytic degradation

Introduction
Metal oxide nanoparticles (NPs) have been commonly used in a wide variety of bio-applications, including diagnostics, drug and gene delivery, cell and tissue engineering and therapeutic uses [1]. MgO is an effective metal oxide and is also commonly used in various fields, such as the manufacture of magnesium batteries, paints, biosensors, and superconductors for catalysis of toxic metal ion sensors, biological activities, remediation of toxic waste, and the refractory material industry [1]. MgO has excellent impressive properties, such as high secondary electron discharge, high melting point, solid microwave absorption power, and because of its non-toxic nature, it also plays an important role in biomedical applications. MgO is widely used in fields such as catalyst supports and insulating oxides with better acid and basic properties [2-3]. Generally, in addition to being biologically synthesized metal NPs through plant mediated pathways. As reducing and capping agents, bio-molecules present in plant extracts work to form stable NPs, Therefore, the characteristics of the metal NPs obtained, including biocompatibility and antibacterial activity and it depends on the characteristics of the different phytochemicals present in the seed extracts from which costly, traditional chemical synthesis methods of NPs face different health and environmental risks as an alternative method [4]. The preparation of metal oxide NPs using plant extracts, plant extract plays a significant interest in rising. In order to obtain the simple, non-toxic and eco-friendly [5]. The present work is intended to synthesis MgO NPs by combustion method using *Cicer arietinum* extract as a fuel for eco-friendly preparation of MgO NPs on a potential commercial scale. Many approaches, such as sol gel technique, pulsed laser deposition, vapor phase oxidation, high temperature solid state synthesis, have been used to synthesize MgO nanoparticles [6, 7]. Commercially available chemicals and naturally occurring compounds are used to prepare MgO NPs as reducing agents [8, 9].

The use of synthetic dyes has been gradually growing in our everyday lives and is being widely researched in the field of carcinogenic dye removal in waste water treatment. Hence, by using an appropriate method of degradation, the removal of extremely carcinogenic dye. One of the most popular techniques is degradation of dyes, using UV light since the reactions are performed cost-effectively and easily under renewable solar energy [10]. Therefore, the present research focuses on antibacterial and photocatalytic dye degradation applications.

Experimental details
Materials
SD Fine chemicals Ltd., Mumbai, purchased the Chemical, Magnesium nitrate. Dry *Cicer arietinum seeds* were obtained from the nearby supermarket.

Preparation of Razma seed extract
Fuel preparation using the seeds of *Cicer arietinum* was carried out and then mechanically ground into powder. The well-grounded powder content has been extracted and the seed powder was added to 500 mL distilled H_2O and conduction at 90^0 C for 20 min and used for the preparation of MgO NPs.

Synthesis of magnesium oxide NPs
In the crucible, 1, 28205 g of magnesium nitrate [Mg $(NO_3)2$ $.6H_2O$] and 10 mL of seed boil extract were added and mixed evenly. The crucible was then put in a pre-heated muffle furnace, held for 25 minutes at a temperature of 500 ± 10^0 C, for combustion. The reaction was finalized within 25 minutes. A pure white material has been obtained. The preparation of NPs was repeated at various seed extract concentrations, such as 5, 20 and 30 mL. The concentration of magnesium nitrate retention was stable at 1.28205 g. For different characterization techniques, the obtained substance was used.

Characterization

Powder XRD data was obtained by (Rigaku smart lab X-ray diffractometer (Cu-Kα λ =1.540 Å) determined the phase purity and crystallite size. (The Cu-Ka λ = 1.540 Å). Using the Bruker Alpha FTIR spectrometer, the FTIR spectrum of the sample was obtained. The optical property was calculated by the perkinelmer Lambda-35 spectrophotometer. The morphology of the MgO NPs was studied by SEM (Gemini- Ultra 55) scanning electron microscopy and chemical composition was evaluated by EDAX.

Procedure for Methylene blue dye photocatalytic degradation

The degradation of Methylene blue (MB) at RT (room temperature) has been performed by the photocatalytic activity using MgO NPs in aqueous solution using a 120 W, 365 nm mercury lamp surrounded by a closed quartz tube as a radiance source of the mercury lamp. 50 mg of MgO photocatalyst was applied into solution of 100 mL by varying the MB dye concentrations (5-20 ppm) in a batch reactor of 150 x 75 mm, maintaining a distance of 18 cm between the radiation source and the reactor. We could find the maximum organization of an adsorption and desorption equilibrium between the MB dye and photocatalyst by this experiment. The glass tube of dye solution including photocatalyst was continuously allowed for stirred in the dark chamber for 30 min. Then, at every 30 min interval, 2 mL of suspension was taken out from the glass tube and their absorbance spectra were observed by UV-Vis spectrophotometer at 665 nm. Centrifugation of the collected solution is very important to obtain the proper absorbance. Using the Beer Lambert law formula, the efficiency of methylene blue dye undergoing degradation was determined.

$$\% \text{ of degradation} = \frac{Ci - Cf}{Ci} \times 100 \ldots\ldots\ldots \quad (i)$$

Ci-dye solution initial concentration and Cf -is final concentration of dye (in ppm). By modifying different parameters such as catalytic load and dye concentration, the photocatalytic experiment was repeated [11].

Antibacterial assay

The process of Agar well diffusion method was used to examine the antibacterial effect of three bacterial strains, such as *Staphylococcus aureus* Gram +Ve bacteria and Gram -Ve *Escherichia coli, Klebsiella aerogenes*. Inaculum was uniformly spread using sterile L- shaped glass rod, nutrient agar plates were prepared and swabbed. Plates were smeared with 100 µl of 24-h mature broth culture of individual bacterial strains. The 6mm diameter holes were made in each petriplate using a sterile cork borer (sterile). And miscellaneous concentration. In order to evaluate its operation, different concentrations of NPs and negative control (1000 and 1500 µg/ well), positive control, ciprofloxacin (5 µg /50 µl) were used, incubating these petriplates for 36 h at 37 ^{0}C .The established inhibition of the bacterial growth was measured in millimeters (mm) from these petriplates, and the results were tabulated in the Table 1. Studies were maintained in triplicates and the average values were determined to estimate the antibacterial effect, are given in table 1 [12].

Results and discussion

XRD structural analysis

X-ray diffraction pattern of MgO NPs is shown in Figure 1. It displays a face-centered cubic structure, following the regular XRD pattern (JCPDS card no: 43- 1022). Using Debye Scherrer's formula, the average crystallite size (D = 14 nm) is determined. The peaks were assigned to (111), (200), (220), (311), and (222) planes at 36.88, 42.75, 62.19, 74.50 and 78.48 respectively, using Scherrer's equation, the mean crystallite size (D) of the particle was determined.

$$D = 0.89\lambda / (\beta \cos\theta) \ldots\ldots\ldots \quad 1$$

Where λ is the Wavelength (Cu Kα), β is full width at half maxima, θ is diffraction angle.

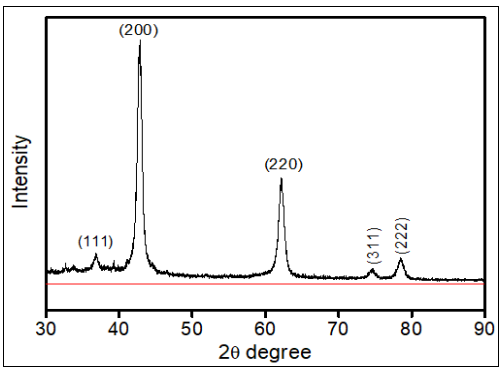

Fig 1: The XRD pattern of MgO nanoparticles

Fourier Transform Infrared spectroscopy analysis of synthesized MgO NPs

FT-IR characterization study, illustrated in Figure 3, showed the surface nature of the MgO NPs. Via the stretching and bending vibrations of -OH by the physically adsorbed H_2O molecule, the wide absorption band was located at 3421 cm^{-1} [13]. It confirms the capping reactions between MgO NPs and the hydroxyl groups of the phytochemicals present in the seed extract. The small double peaks at 2918 and 2854 cm^{-1} are taken into account for C-H stretching vibrations of the CH_2 group, The prominent peak at 1379 cm^{-1} is assigned to Mg-O vibration [14], while the band at 1056 is the characteristic peak of different modes of C-O and C-O-C diagnostic bonds, respectively. The cubic phase of MgO NPs confirms a band located at 862 cm^{-1} [15]. The band at 430 is a result of MgO stretching vibration.

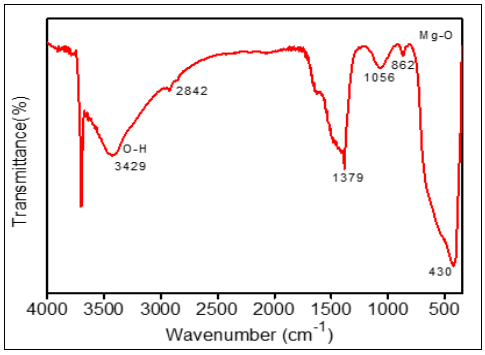

Fig 2: FTIR spectrum of MgO NPs

Morphological studies

As shown in figure 3, the MgO NPs Scanning Electron Microscopy (SEM) images. The photos displayed an agglomerated spong-like structure and were spread evenly over the material surface to present a broad surface area to volume ratio. The elemental analysis of MgO NPs has been further confirmed by the EDAX spectrum, while Figure 4, and shows the EDAX spectrum of MgO NPs. Which confirms the high intensity 1:1 atomic ratio presence of Mg and O in the prepared sample, as observed in pure MgO NPs.

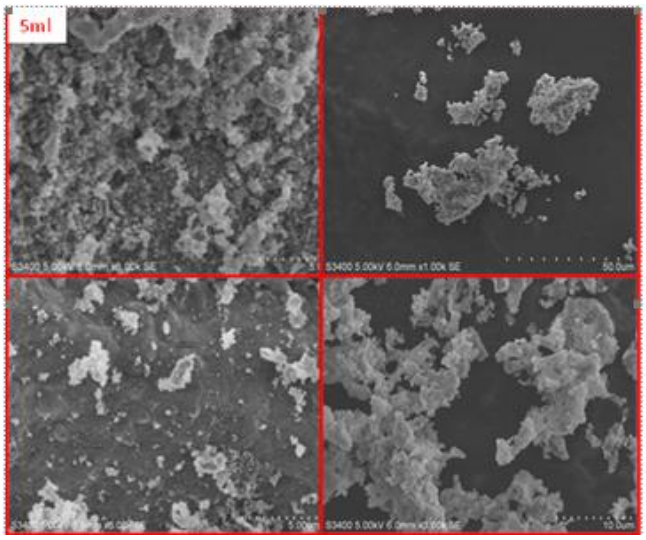

Fig 3: SEM image of MgO nanoparticles

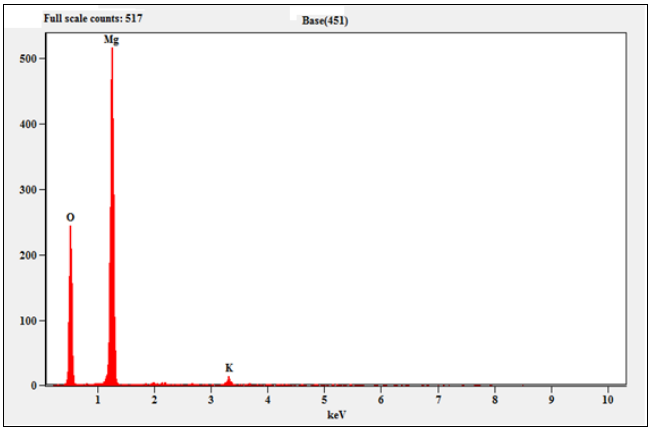

Fig 4: EDAX image of MgO nanoparticles

Optical studies

UV- DRS studies

As shown in Figure 2, UV- DRS spectrum of synthesized MgO nanoparticls. The MgO NPs of the DRS spectrum consist of Diffuse Reflectance Spectra (DRS) absorption. Due to the large absorption peak host lattice, the strong band in the spectrum is located at the wavelength of 240 nm area. The theory of Kubelka-Munk (K-M) is effectively demonstrated in order to assess the energy band gap (Eg) of prepared MgO NPs from DR spectra. DRS plot drawn to the plots of [F (R∞) hν] $^{1/2}$ vs. photon energy hν about the intercept of the tangents. The energy band gap value of MgO NPs at 4.97 eV is given by the tangent intercept on the X axis. The decrease in the energy band gap (red shift) compared to bulk MgO (7.8 eV) was notable.

The phenomenon of quantum confinement is behind in increase in crystallite size, which also entails reducing the value of the Eg value takes place due to the expansion of the crystal lattice and weakening of the inter-atomic bonds. Less energy was required for the weaker bonds to break down and easily excite the valence band electron to the conduction band. The photo energy (hν) and function F (R∞) of Kubelka-Munk were determined using the following equations [16].

$$F(R\infty) = \frac{(1-R\infty)2}{2R\infty} \quad \text{----------} \quad 1$$

$$h\nu = \frac{1240}{\lambda} \quad \text{----------} \quad 2$$

λ: absorption wavelength, R∞; reflection coefficient of the sample.

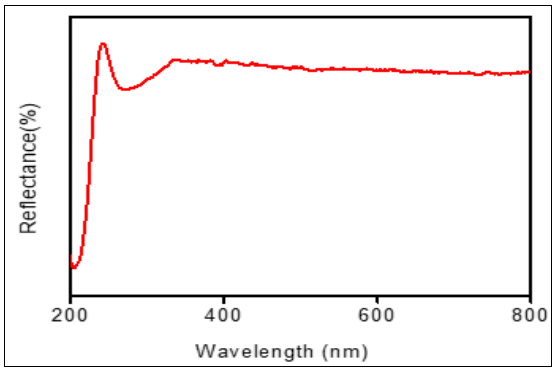

Fig 5: UV-DRS spectra of MgO NPs

Photocatalytic degradation studies

Catalytic load effect on photocatalytic activity

Figure. The effect of catalytic loading by photocatalytic degradation of MB dye is explained in 6. The optimal catalyst quantity was defined by varying the catalytic load from 10 mg to 40 mg/100 mL. The active sites on the catalytic load surface increase to 40 mg/100 mL as the volume of the catalyst increases and the catalytic load also increases further. Due to the creation of an opaque solution that suppresses light transmission to superoxide and free hydroxides this causes a decrease in efficiency. By all the above discussed mechanism, 40mg/100ml has been provided higher degradation of MB dye for good catalyst load.

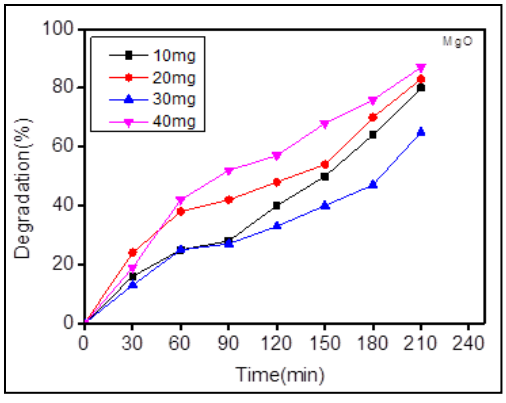

Fig 6: Percentage of MB degradation under different catalytic loads of nanoparticles (10, 20, 30, 40 mg) at UV-light exposure.

Influence by the concentration of MB dye

Figure 7: demonstrates the influence of MB dye concentration on the photocatalysis of MgO NPs. In the experiment, the MB dye ranged from 5-20 ppm in the concentration range. Until this experiment, 0.4 g and 10 pH were kept constant at the set catalytic load. As the dye quantity rises, the time required for the completion of the MB dye concentration increases by 5 to 20 ppm. As the concentration of dye increases, several dye molecules get adsorbed on the catalyst surface, this leads to decreased active sites on the catalyst. The availability of less superoxide and hydroxyl radicals limits light penetration [17].

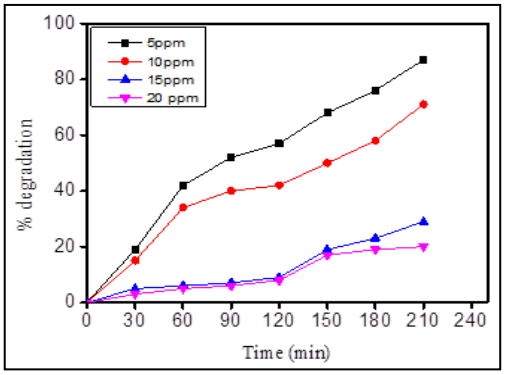

Fig 7: Effect of dye methylene blue concentration on MgO NPs

Antibacterial activity

The antibacterial effects of MgO NPs are as shown in Figure 8. The agar well diffusion method, was tested by exposing Gram + Ve *(S.aureus*) and Gram - Ve *(Klebsiella aerogenes* and *Escherichia coli*) bacterial strains. The highly inhibition activity is shown by *K. Aerogenes* (1.67±0.33) and *S.aureus* (2.00±0.00), and lowest antibacterial effect is shown by *E.coli* (1.00±0.00). ROS formation, lipid peroxidation and electrostatic interaction of NPs with bacteria are the primary reasons for the bactericidal effect of MgO NPs. They seriously damage the membrane of the bacterial cell, resulting in the inhibition of cell growth and cell death occurs. Nanoparticles can be physically bactericidal to a cell membrane as they come in contact with the bacterial cell membrane [18]. Zone of inhibition results indicated in table 1.

Table 1: Inhibition zone of MgO NPs against the pathogenic bacterial strains tested

Sl. No		*S.aureus*	*K.aerogenes*	*E. coli*
(5µg/50 µl)	Standard	12.87± 0.33	11.68±0.33	8.45±0.33
(500µg/50 µl)	MgO NPs	0.70± 0.00	1.30 ±0.00	0.57±0.17
(1000µg/100µl)	MgO NPs	2.30 ±0.00	1.47 ±0.33	1.00±0.00

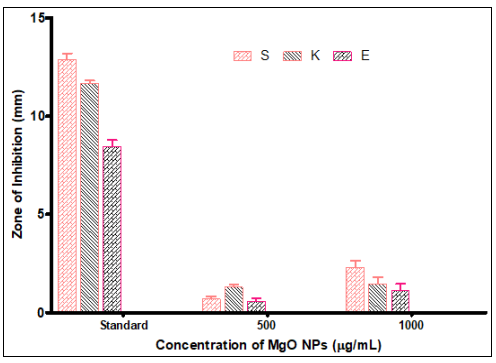

Fig 8: ZOI of MgO NPs

Conclusion

In the present work, using *Cicer arietinum* seed extract, we have successfully prepared MgO NPs by solution combustion technique. XRD, FTIR, and SEM with EDAX, were defined by the MgO NPs prepared. Powder X-ray diffraction analysis revealed that a crystallite size of 14 nm on average, the nanostructures composed of cubic- phase MgO. The formation of agglomerated sponge like structure by SEM is supported by surface morphological analysis. The prepared MgO NPs shows a good antibacterial activity and photocatalytic activity in the direction of MB dye photocatalytic degradation.

References

1. Karthik K, Dhanuskodi S, Prabu kumar S, Gobinath C, Sivaramakrishnan. Microwave assisted green Synthesis of Mgo nanorods and their antibacterial and anti-breast cancer activities. Materials Letters. 2017; 206:217–220.
2. Xue-Nan GU, Yu-Feng Zheng. Front. A review on magnesium alloys as biodegradable materials. Mater. Sci. China. 2010; 4:111–115.
3. Liang SH, Gay ID. A 13C solid –state NMR study of the chemisorptions and decomposition of ethanol on MgO. Journal of Catalysis. 1986; 101:293-300.
4. Mohanraj R. Antimicrobial activities of metallic and metal oxide nanoparticles from plant extracts. In: Grumezescu, A.M. (Ed.). Antimicrobial nano architectonics from synthesis to applications. Elsevier, New York, 2017, 83-100
5. Jhansi K, Jayarambabu N, Reddy KP, Reddy NM, Suvarna RP, Rao KV, *et al.* Biosynthesis of MgO nanoparticles using mushroom extract: effect on peanut (Arachis hypogaea L.) seed germination. 3 Biotech, 2017, 7- 263.
6. Mirzaei H, Davoodnia A. Microwave assisted sol- gel synthesis of MgO NPs and their catalytic activity in the synthesis of hantzsch 14- dihydropyridines Chin. J. Catal, 2012, 33:1502
7. Okitsu K, Mizukoshi y, Yamamoto TA, Maeda Y. Sonochemical synthesis of gold Nps on chitosa Lett. Mater. 2007, 61:3429
8. Ganapathi Rao K, Venkateswara Rao K. Eco- friendly synthesis of MgO NPs from orange fruit waste Int. J. Adv. Res. Phys. Sci, 2015, 21.
9. Bai J, Meng F, Wei C. Solution combustion synthesis and characteristics of nanoscale MgO powders Ceram-Silik, 2011, 55-20
10. Ravishankar RV, jamuna B. Nanoparticles and their potential application as antimicrobials science Against Microbial pathogens (Communicating current Research Technological Advances) ed A Mendez –Vilas (Badajoz: Formatex), 2011, 197-209.
11. Suresh D, Nethravathi PC, Udayabhanu, Pavan Kumar MA, Raja Naika H, Nagabhushana CH, *et al*. Chironji mediated facile green synthesis of ZnO nanoparticles and their photoluminescence, photodegradative, antimicrobial and antioxidant activities. Materials Science in Semiconductor processing. 2015; 40:759-765.
12. Perez C, Paul M, Bazerque P. An antibiotic assay by the agar well- diffusion method Acta. Med. Exp, 1990, 15113
13. Ravishankar RV, Jamuna B. Nanoparticles and their potential application as antimicrobials science Against

Microbial pathogens (Communicating current Research Technological Advances) ed A Mendez-Vilas (Badajoz: Formatex), 2011, 197-209
14. Enobong R, Essien Violette N, Atasie, Anastecia O, Okeafor. Biogenic synthesis of magnesium oxide nanoparticles using Manihot esculenta (Crantz) leaf extract. International Nano Letters. 2020; 10:43-48
15. Reddy Yadav LS, Lingaraju K, Manjunath K, Raghu GK, Sudheer Kumar KH, Nagaraju G, et al. Synergistic effect of MgO nanoparticles for electrochemical sensing. Mater. Res. Express. 2017; 4:025028.
16. Udayabhanu Nagaraju G, Nagabhushana RB, Basavaraj Raghu GK, Suresh D. Green, non-chemical route for the Synthesis of ZnO superstructures, Evaluation of its applications towards Photocatalysis, Photoluminescence and Bio- sensing. ACS Publications, Crystal Growth and Design is published by the American Chemistry Society, 2016, 1155.
17. Pavitra V, Udayabhanu Harini R, Viswanatha R, Praveen B, Praveen M. Snochemical synthesis of SnO_2-CuO nanocomposite: diverse applications on Li- ion battery, electrochemical sensing and photocatalytic activity. Journal of Materials Science: Materials in Electronics, 2020, 8737-8749
18. Suresh J, Yuvakkumar R, Sundrarajan M, Hong SI, Green synthesis of magnesium oxide NPs Adv, Mater, Res, 2014, 952141